

 Open access • Posted Content • DOI:10.1101/795088

A decoy heterotrimeric G α protein has substantially reduced nucleotide binding but retains nucleotide-independent interactions with its cognate RGS protein and G $\beta\gamma$ dimer — [Source link](#)

Fei Lou, Tigran M. Abramyan, Haiyan Jia, Alexander Tropsha ...+1 more authors

Institutions: University of North Carolina at Chapel Hill

Published on: 06 Oct 2019 - bioRxiv (Cold Spring Harbor Laboratory)

Topics: Heterotrimeric G protein, G protein, Homology modeling, Nucleotide and Microscale thermophoresis

Related papers:

- [Structure of G \$\alpha\$ i1 Bound to a GDP-Selective Peptide Provides Insight into Guanine Nucleotide Exchange](#)
- [Insights regarding guanine nucleotide exchange from the structure of a DENN-domain protein complexed with its Rab GTPase substrate.](#)
- [Insights into the Molecular Activation Mechanism of the RhoA-specific Guanine Nucleotide Exchange Factor, PDZRhoGEF](#)
- [Electrostatic control of GTP and GDP binding in the oncoprotein p21ras](#)
- [Structure of the RGS-like domain from PDZ-RhoGEF: linking heterotrimeric g protein-coupled signaling to Rho GTPases.](#)

Share this paper:    

View more about this paper here: <https://typeset.io/papers/a-decoy-heterotrimeric-ga-protein-has-substantially-reduced-1gavqcc0l>

1 Correspondence: Dr. Alan M. Jones

2 Address: Department of Biology

3 The University of North Carolina at Chapel Hill

4 Coker Hall, CB#3280

5

6 Phone : (919) 962-6932

7 Fax: (919) 962-1625

8 E-mail: alan_jones@unc.edu

9

10 The author responsible for distribution of materials integral to the findings presented in this article is Dr.

11 Alan Jones alan_jones@unc.edu

12 **Running Title: Atypical Heterotrimeric G Proteins**

13 **Keywords:** Arabidopsis, AGB1, G $\beta\gamma$, AtGPA1, AtRGS1, Extra-large G protein, XLG2, dominant

14 negative G alpha

15

A decoy heterotrimeric G α protein has substantially reduced nucleotide binding but retains nucleotide-independent interactions with its cognate RGS protein and G $\beta\gamma$ dimer

Fei Lou^a, Tigran M. Abramyan^b, Haiyan Jia^a, Alexander Tropsha^b, and Alan M. Jones^{a,c*}

Departments of ^aBiology and ^cPharmacology, University of North Carolina at Chapel Hill, NC, U.S.A.

^bDivision of Chemical Biology and Medicinal Chemistry, UNC Eshelman School of Pharmacy, University of North Carolina at Chapel Hill, NC, USA.

*Correspondence: Dr. Alan M. Jones email, alan_jones@unc.edu

ABSTRACT

Plants uniquely have a family of proteins called extra-large G proteins (XLG) that share homology in their C-terminal half with the canonical G α subunits; we carefully detail here that Arabidopsis XLG2 lacks critical residues requisite for nucleotide binding and hydrolysis which is consistent with our quantitative analyses. Based on microscale thermophoresis, Arabidopsis XLG2 binds GTP γ S with an affinity 100-1000 times lower than that to canonical G α subunits. This means that given the concentration range of guanine nucleotide in plant cells, XLG2 is not likely bound by GTP *in vivo*. Homology modeling and molecular dynamics simulations provide a plausible mechanism for the poor nucleotide binding affinity of XLG2. Simulations indicate substantially stronger salt bridge networks formed by several key amino-acid residues of AtGPA1 which are either misplaced or missing in XLG2. These residues in AtGPA1 not only maintain the overall shape and integrity of the apoprotein cavity but also increase the frequency of favorable nucleotide-protein interactions in the nucleotide-bound state. Despite this loss of nucleotide dependency, XLG2 binds the RGS domain of AtRGS1 with an affinity similar to the Arabidopsis AtGPA1 in its apo-state and about 2 times lower than AtGPA1 in its transition state. In addition, XLG2 binds the G $\beta\gamma$ dimer with an affinity similar to that of AtGPA1. XLG2 likely acts as a dominant negative G α protein to block G protein signaling. We propose that XLG2, independent of guanine nucleotide binding, regulates the active state of the canonical G protein pathway directly by sequestering G $\beta\gamma$ and indirectly by promoting heterodimer formation.

42 INTRODUCTION

43 The canonical heterotrimeric guanosine nucleotide-binding protein complex, consisting of $G\alpha$, $G\beta$ and
44 $G\gamma$ subunits, serves as a molecular on-off switch in the cell. The inactive or “off-state” form consists of
45 the guanosine diphosphate (GDP) bound to the $G\alpha$ subunit in complex with the $G\beta\gamma$ dimer. For the
46 active or “on-state”, exchange of GDP for GTP in $G\alpha$, either spontaneously or catalyzed by a guanine
47 nucleotide exchange factor, changes the $G\alpha$ conformation leading to dissociation, partly or entirely (1),
48 from the $G\beta\gamma$ dimer and thus enabling both $G\alpha$ and $G\beta\gamma$ to propagate signaling to downstream
49 components (2-4). Signaling is terminated when the $G\alpha$ subunit hydrolyzes GTP thus returning to the
50 inactive GDP-bound state. The rate of GTP hydrolysis is an intrinsic property of each $G\alpha$ subunit but it
51 can be accelerated by Regulator of G protein Signaling (RGS) proteins (5, 6). The $G\alpha$ structure required
52 for nucleotide binding and hydrolysis and for interaction with $G\alpha$ - $G\beta\gamma$ and $G\alpha$ -RGS interactions are well
53 understood (7, 8).

54 In humans, there are multiple genes encoding G protein subunits resulting in 23 $G\alpha$, 5 $G\beta$ and 12
55 $G\gamma$ subunits. The $G\alpha$ subunits are divided into four subclasses (G_s , G_i , G_q and $G_{12/13}$) based on
56 function and sequence similarity. However, in Arabidopsis, there is only one canonical $G\alpha$ (AtGPA1)
57 which approximates the sequence of the ancestral $G\alpha$ subunit that evolved into these four animal $G\alpha$
58 subclasses (9). AtGPA1 has a near identical structure to that of human $G_{i\alpha 1}$ (10). In addition to the
59 canonical $G\alpha$ subunit AtGPA1, the Arabidopsis genome encodes three atypical Extra-large G proteins
60 (XLG1, XLG2, and XLG3) (11). The other components of the Arabidopsis G protein core are a $G\beta$
61 subunit (AGB1) (12), one of three $G\gamma$ subunits (AGG1, AGG2, and AGG3) (13), and one receptor-like
62 RGS protein (AtRGS1) (14).

63 The presence of these atypical G proteins makes G protein signaling in plants unique and
64 paradoxical (11, 15, 16). Specifically, the N-terminal half of XLG proteins lacks homology to any
65 characterized domain but contains a putative nuclear localization signal and a cysteine-rich region while

66 the C-terminal half of XLG proteins shares homology (i.e. evolutionary history, (16)) with canonical G α
67 subunits (~30% identity). However, there is controversy to what extent that these atypical G α homologs
68 bind and hydrolyze nucleotides and interact with AtRGS1 and AGB1 (17, 18).

69 For canonical G α subunits, there are three major conformational changes between the GDP and
70 GTP-bound states of the protein located in what are called Switch I, II and III. Switch I and Switch II
71 directly contact the bound guanine nucleotide and include residues critical for catalyzing GTP hydrolysis,
72 while Switch III contacts Switch II when in the activated conformation (19). These switches are linked
73 between the nucleotide-binding domain and the RGS binding domain and are represented by five
74 conserved sequence motifs named G1 to G5 (20). The G1–G3 boxes provide critical contacts for the
75 β and γ phosphates of the guanine nucleotide and are essential for the coordination of Mg²⁺. The G4
76 and G5 loops are involved primarily in binding the guanine ring. The G2 and G3 boxes overlap with
77 Switches I and II that are also the key G $\beta\gamma$ binding sites. The RGS domain directly binds to the three
78 switch regions and stabilizes them in a transition state conformation.

79 It is paramount to resolve unequivocally if XLG proteins bind guanine nucleotide and relevant
80 signaling elements such as RGS and G $\beta\gamma$ to elucidate its atypical mechanism. Here, we combine
81 structure-based and physicochemical experimental methods along with molecular simulations to
82 analyze the binding of XLG2 with both the nucleotide and with a candidate binding partner, AtRGS1/
83 G $\beta\gamma$ dimer. We describe for the first time in great detail the structural issues that should raise concern
84 among those who claim that XLG proteins are nucleotide-dependent switches. In fact, we show that
85 XLG2 binds nucleotide so poorly that it is essentially nucleotide free in the cell, yet despite its
86 nucleotide-free, “empty” state, XLG2 interacts with its partners AtRGS1 and AGB1 with an affinity
87 similar to AtGPA1 in its transition state. We used molecular dynamic simulations to explain how this
88 binding is disrupted and how these protein-protein interactions are maintained.

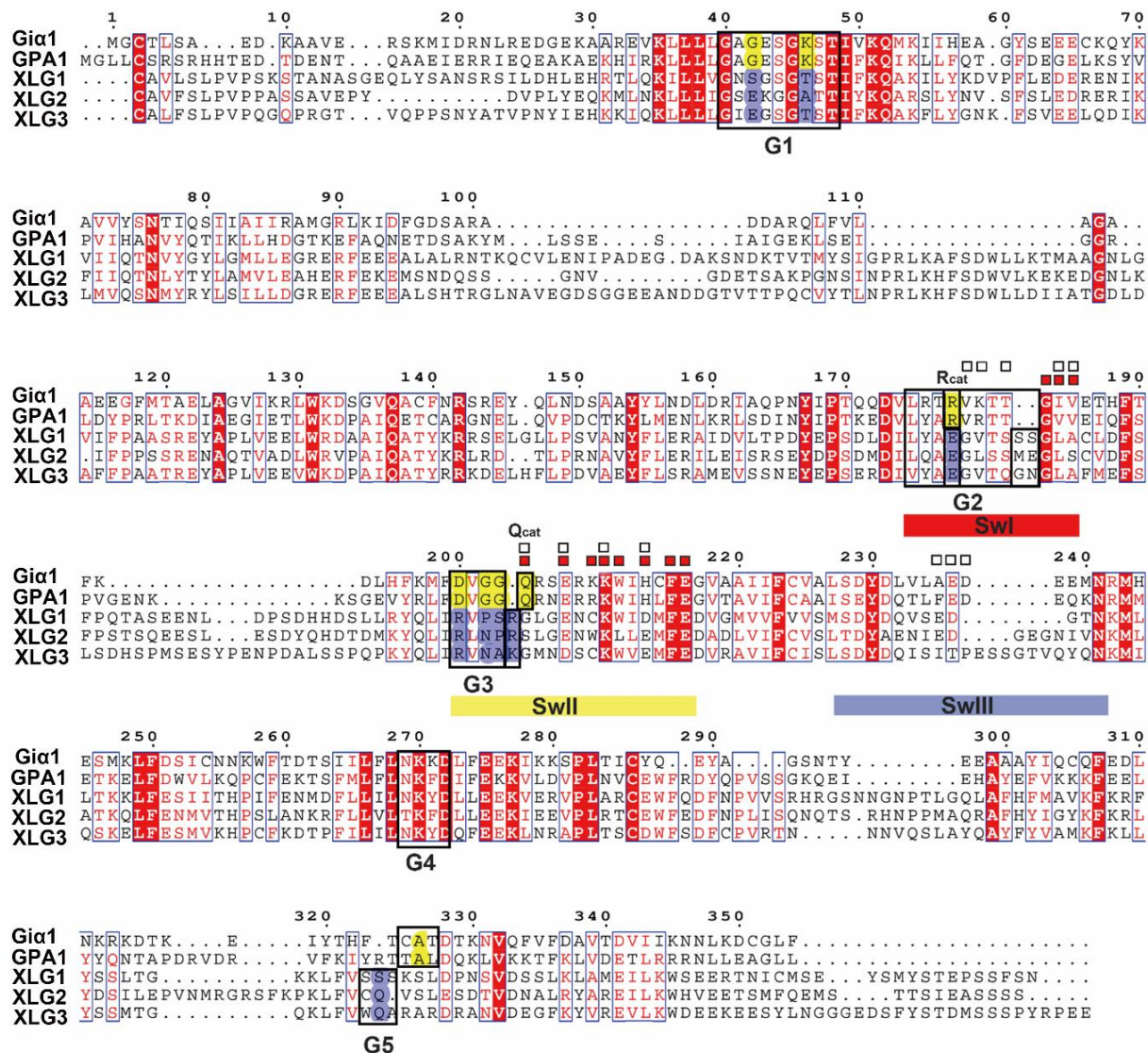
90 RESULTS AND DISCUSSION

91 **XLG proteins lack critical residues for coordination of the γ and β phosphates on the guanine** 92 **nucleotide**

93 A multiple sequence alignment of XLGs G α domain, AtGPA1, and human G α 1 is shown in Fig. 1 with
94 the G1-G5 motifs and switches I-III regions highlighted (noted as SwI-III). To compare the protein
95 structures between XLGs and canonical G α subunits, we created high-quality models of the G α
96 homology domains of XLG2 using MODELLER and the aligned sequences shown in Fig. 1. The human
97 RGS4 and G α 1 transition state (Ligand: AlF₄ and GDP) complex (PDB [1AGR]) was used as template
98 to generate the models of XLG2. Models were created using the *Automodel* script based on the
99 template of human G α 1 in complex with AlF₄ and GDP (PDB [1AGR]). For evaluation and selection of
100 the "best" model, we calculated the objective function (molpdf) DOPE score, GA341 assessment score
101 between the model and the template (Fig. S1). The final model (XLG2-1) was selected given the lowest
102 average value of the molpdf and the DOPE assessment scores.

103 As shown in Fig. S2, human G α 1 and Arabidopsis GPA1 have two domains: a Ras-like domain
104 and an all-helical domain. Animal G α subunits and AtGPA1 are extremely similar in structure (RMSD=
105 1.8 Å (10)). The Ras-like domain is essential for the nucleotide and RGS proteins binding which
106 contains the five guanine nucleotide binding motifs (G1-G5) and three flexible switch regions (SwI-III)
107 (Fig. S2A). The all-helical domain is important for the intrinsic nucleotide exchange rate (21, 22). XLG2-
108 1 shares a similar overall 3D structure with human G α 1 and AtGPA1 even though the sequence identity
109 is ~ 30%. XLG2-1 contains a globally similar Ras-like domain and α helix domain. The three switch
110 regions and the G1-G5 boxes are highlighted (Fig. S2B). The RMSD between G α 1 and XLG2-1 is 0.67
111 Å. However, despite similar global structure between XLG2-1 and human G α 1, many of the conserved
112 motifs which are essential for nucleotide binding and hydrolysis are missing, including key residues
113 within the G1, G3 and G5 motifs for nucleotide binding and some dominant residues in the P loop,

114 Switch I and Switch II for coordinating water and Mg²⁺ to catalyze GTP hydrolysis (Fig. 1 and Fig. 2B).
 115 These critical differences between the canonical G α and the XLG G α domain are described in detail
 116 next.



117

118 **Figure 1. Alignment between human *Gia1* Arabidopsis *AtGPA1* and the C terminal G alpha domain**
 119 **of the three XLGs** The G1-G5 motifs are shown in black boxes. The switches I-III regions (SwI-III) are
 120 highlighted (SwI in red, SwII in yellow and SwIII in blue). A percentage of equivalent residues is calculated per
 121 columns, considering physico-chemical properties. Blue boxes highlight residues with the same physico-
 122 chemical properties and red solid highlighting means the same residues. The contact residues to RGS protein
 123 are labeled with white boxes □ and the contact residues with G β are labeled with red boxes ■. The residues
 124 which are conserved in human *Gia1* and *AtGPA1* for GTP/GDP binding and hydrolysis but are missing in XLGs
 125 are highlighted with yellow and blue respectively. The residues essential for the catalysis of the nucleotide are
 126 highlighted as Rcat and Qcat. (The C domain of XLGs start with first C residues in the paper, C436 in XLG1,
 127 C435 in XLG2 and C396 in XLG3).

128 The highly conserved G1 motif is a phosphate-binding region containing a flexible structure designated
129 “P-loop” (23). The G1 motif has a consensus sequence of GXXXXGKS/T for the heterotrimeric G α
130 subunits (7). The P-loop envelopes the phosphates allowing the main chain and side-chain nitrogen
131 atoms to interact tightly with the negatively-charged phosphates (Fig 2 A, B). In animal G α subunits as
132 well as in AtGPA1, the sequence in the P loop and G1 motif are invariantly set to “GAGESGKS” (Fig 1,
133 see G1 box). However, in XLG2-1, the G42 residue of G α 1 in the P loop is replaced by E471 and the
134 K46 residue of G α 1 is replaced by A475, respectively (Fig 1 and Fig 2B). The G42 residue of G α 1 or
135 G47 residue of AtGPA1 in the P loop play a dominant role in binding the substrate with the main chain
136 forms hydrogen bond with the γ phosphate oxygen atom (23). This G residue is shown in Fig 2A and
137 B. More importantly, only a G residue side chain is small enough to avoid steric clash with the nucleotide
138 and mutation of the corresponding P-loop residue in G α 1, G42 to V, also drastically reduces its GTP
139 hydrolysis activity (24-26). Structural studies of G42V mutant in G α 1 suggest that the introduced valine
140 side chain sterically prevents appropriate positioning of Q204 which coordinates a nucleophilic water
141 molecule during GTP hydrolysis and steric pressure will induce the reconfiguration of switch II (6, 25,
142 26). Thus, we assume that the substitution of the large side chain of E471 in XLG2-1 reduces GTPase
143 activity (Fig 2B).

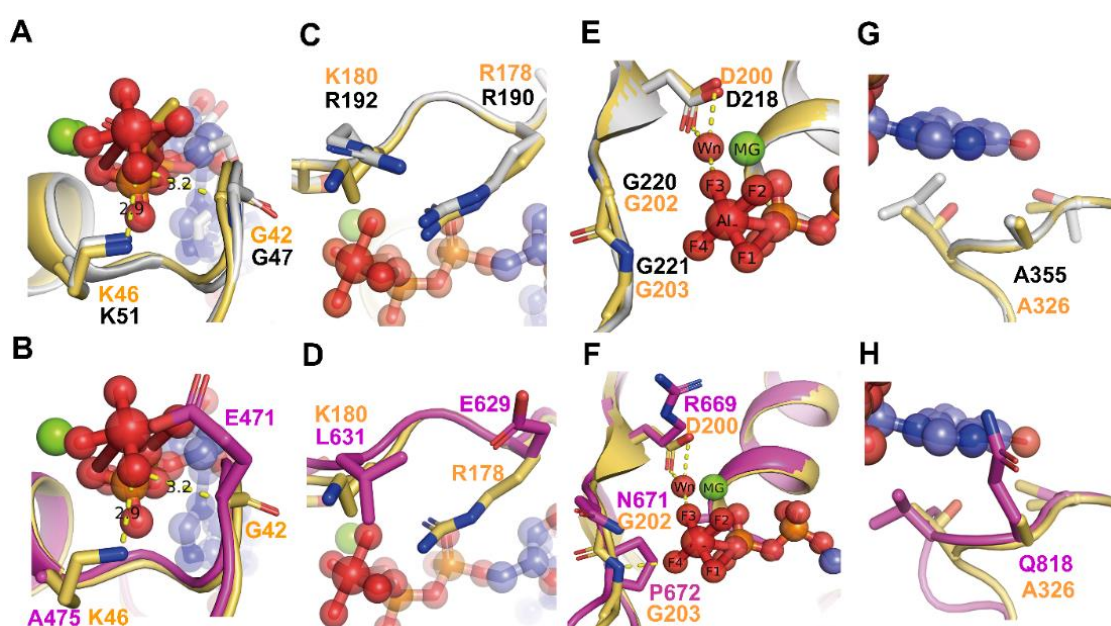


Figure 2. Comparison of the G motifs of AtGPA1 PDB [2XTZ] and the XLG2 G alpha domain model with human G α 1 (PDB [1AGR]) Grey: AtGPA1, Magenta: XLG2-1 model, Light orange: G α 1. The substrate GDP and AlF₄ are shown as sticks and spheres. Mg²⁺ is shown as green sphere. Wn: nucleophilic water. The main different residues in G1 motif of XLG2 compared with G α 1 and AtGPA1 are shown as sticks (**A, B**). Both AtGPA1 and G α 1 have the same G and K residues in G1 motif (**A**). the G42 and K46 in G α 1 were replaced by E471 and A1475 in the counterpart position of XLG2 (**B**). The main different residues in G2 motif of XLG2 compared with G α 1 and AtGPA1 are shown as sticks (**C, D**). Both AtGPA1 and G α 1 have the same R residues (known as arginine finger) and similar charged K180 and R192 in G2 motif (**C**). But in XLG2 no arginine finger exists rather a Glu is at this position. Also, the charged K or R was replaced by a L (**D**). The main different residues in G3 motif of XLG2 compared with G α 1 and AtGPA1 are shown as sticks E, F. Both AtGPA1 and G α 1 have the same DVGG residues in G3 motif (**E**). But in XLG2 the DVGG was replaced by R669/N671/P672 relatively (**F**). The main different residues in G5 motif of XLG2 compared with G α 1 and AtGPA1 are shown as sticks in G and H. Both AtGPA1 and G α 1 have the same A residues in G5 motif (**G**). While in XLG2 the conserved A was replaced by Q818 (**H**).

Additional differences were found with the P loop of the XLG proteins. The lysine (K46 of G α 1 and K51 of AtGPA1) residue in the G1 motif directly interacts with the β - and γ -phosphate oxygens of the GTP and thus is crucial for the required free energy change (ΔG) (Fig. 2A). Given that there are two dominant residues mutations in the nucleotide pocket of XLG2 (G42 in G α 1 to E471 and K46 to A475) (Fig. 3B), we hypothesize that XLG2 binds the nucleotide with a reduced affinity *in vitro* and that XLG2 is nucleotide free *in vivo*.

The G3 box contains the signature sequence DXGG conserved throughout the heterotrimeric G-protein superfamily. Similar to the P loop, residues with the G3 motif interact with the γ -phosphate of GTP but also orients the Mg²⁺ ion that is critical for coordination of the guanine nucleotide. In AtGPA1 and G α 1, the G3 box is invariant “DVGG” (Fig. 2E), however in the XLG2 G α domain, the residues are replaced by “RLNP” (Fig. 2F). The conserved Asp residue of canonical G α subunits provides the water-molecule-mediated coordination of Mg²⁺ and therefore, the substitution of Asp for this critical Arg disrupts the ability to bind Mg²⁺ (6, 7, 27). Moreover, the main chain amide of the signature Gly residue is essential for nucleotide binding through hydrogen bonding to the γ -phosphate oxygen of the GTP (27). The main chain amide of this Gly is hydrogen bonded to the γ -phosphate and mutation of the two Gly residues in the G3 box confer dominant negative phenotypes (7, 27, 28). Gilman’s group showed that GDP-bound G α s G226A mutant (the second Gly in the G3 DVGG motif) has a higher affinity for

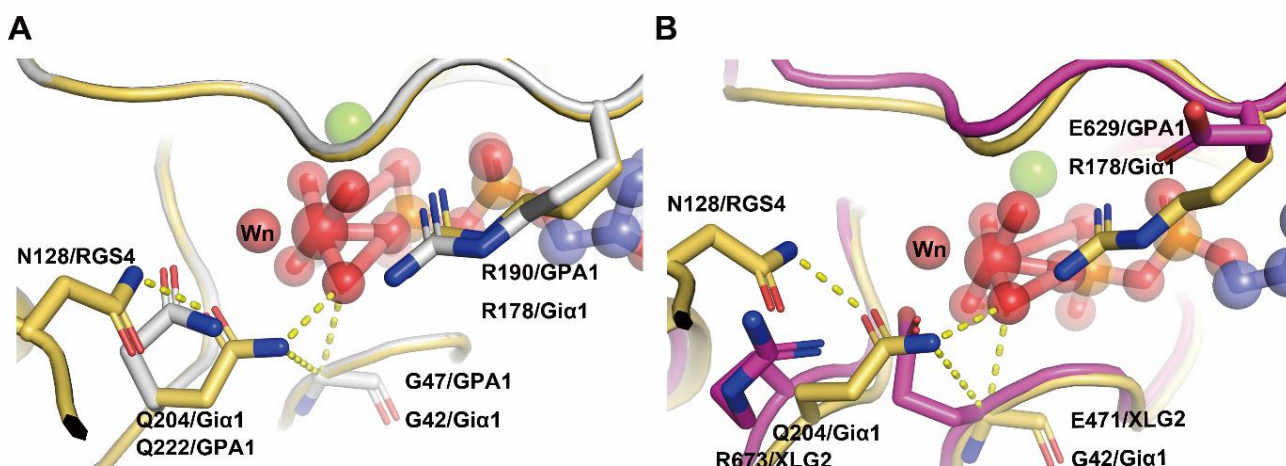
177 G β than the wild-type subunit and is incapable of undergoing a GTP-induced conformational change
178 (29). Taken together, stark differences in the three dominant residues in the G3 motif in the XLG2
179 protein nucleotide binding pocket which is conserved among all XLG proteins (Fig. 1) suggest that
180 XLGs exist in the empty nucleotide state.

181 The G5 motif consensus is S/C/T-A-K/L/T. In Gi α 1, the G5 motif sequence is C-A-T (A = residue
182 326) and in AtGPA1, it is T-A-L (A = residue 355, Fig. 2G and H). In either form, the main chain of
183 A326 in Gi α 1 is essential for the binding of GTP/GDP specifically forming a hydrogen bond with the
184 oxygen of the guanidine nucleotide and S substitution at this site weakens the affinity for GTP γ S
185 through steric crowding (30). Also, the equivalent A366S mutation in the G5 motif of Gas decreases
186 Gas's affinity for GDP and GTP γ S by steric crowding and shifting G α towards the empty nucleotide
187 pocket state (30, 31). However, in XLG2, the equivalent residues are C-Q-V (Q = residue 818, Fig. 2H).
188 Thus, this substitution of A326 with Q818 in XLG2-1 is predicted to create a steric clash for nucleotide
189 binding providing further inference that XLG is nucleotide-free.

191 **XLG proteins lack key residues to catalyze GTP hydrolysis**

192 Two amino acids, one from the G α subunit (the conserved catalytic glutamine residue in Switch II region
193 which is named "Qcat") and one from the RGS protein (the so-called "Asn thumb"), together with
194 nucleophilic water and a Mg²⁺ in the catalytic center are essential elements for the catalytic reaction (6)
195 (Fig. 3). In Gi α 1, the Qcat in Switch II is Q204 is essential for catalytic activity in the G α subunit. A
196 conserved Arg residue in Switch I region designated "Rcat" here, is also a major determinant of the
197 catalytic activity. A water molecule designated "Wn" occupies the position for the nucleophile engaged
198 in an in-line attack on the phosphate. The Asn thumb (N128 in RGS4) in the RGS domain reorients the
199 Qcat allowing the carboximido moiety to form hydrogen bonds with AlF₄ mimicking a γ phosphate
200 oxygen atom and Wn. Rcat forms electrostatic interactions with the β phosphate oxygen and with one

201 of the fluoride substituents of AlF_4 (Fig.3). Mutations in these residues of Switch I and Switch II are
202 known to drastically alter GTPase activity (6).



203

204 **Figure 3. Interactions between the catalysis center of the Ras domain and critical residues of RGS**
205 **proteins. (A)** The critical contact residues between Gai1 and RGS4 (PDB 1AGR) are shown in light orange. Arg
206 178 (Rcat) is within hydrogen bonding distance of the leaving group β - γ bridge oxygen and Q204 (Qcat) is a
207 hydrogen bond donor to a fluorine (or O⁻) Al substituent and accepts a hydrogen bond from the presumptive
208 water nucleophile (Wn). The hydrogen bond network (yellow dashed lines) involving N128 (Asn thumb of RGS4),
209 Qcat, G42 and the the γ phosphate (modeled by AlF_4) orient Wn for nucleophilic attack and stabilize developing
210 charge at the β - γ bridge leaving group oxygen. RGS4 residues Asn 128 constrain the conformation of Gai1 Q204
211 (Qcat) to the pre-transition state conformation. AtGPA1 contains the same catalysis network (A) however the
212 catalysis network was disrupted in XLG2 with the loss of the Gln_{cat} and Arg finger and replaced by R673 and
213 E629 respectively (B). Grey: AtGPA1, Magenta: XLG2, Light orange: Gai1. The substrate GDP and AlF_4 are
214 shown as sticks and spheres. Main catalysis residues between Gai1, AtGPA1, XLG2 and RGS4 are highlighted
215 as sticks. Wn: nucleophilic water.

216

217 All XLG proteins lack both essential Rcat and Qcat for the catalysis (Fig. 3B). In XLG proteins, the
218 Rcat residue in Switch I is E, creating a charge reversal that disrupts electrostatic interactions with the
219 β and γ phosphates of the guanine nucleotide. The equivalent mutation in Gai1 exist as a stable protein
220 in a nucleotide-free state and lacks the capacity to form the active conformation (19). In all XLG proteins,
221 the Qcat residue of Switch II is R/K which is unable to coordinate with either the Asn thumb of the RGS
222 protein or the nucleophilic water to hydrolyze GTP. Both Q204R and R178C mutations abrogate
223 nucleotide hydrolysis (19). The structural characteristic of the XLG proteins catalysis center suggests

224 that XLGs lack the ability both to coordinate with RGS to hydrolyze GTP and the intrinsic GTPase
225 activity of G γ subunits.

226

227 **XLG2 has a much lower binding affinity towards nucleotide than canonical G subunits yet**
228 **interacts with similar affinities towards G $\beta\gamma$ and AtRGS1**

229 Assessments of nucleotide binding to XLG proteins to date lack quantitation for binding constants (32).
230 Similarly, XLG protein interaction with AtRGS1 and G $\beta\gamma$ have been indirect measurements (11, 16, 17).
231 To correct this deficit, we used microscale thermophoresis (MST) to measure the binding affinity of
232 XLG2 and AtGPA1 with guanine nucleotides (GDP and GTP γ S) and with binding partners AtRGS1 and
233 G $\beta\gamma$. The advantages of this new technique are the capability of obtaining accurate affinities in the low
234 affinity (μ M-mM Kd) range with small amounts of protein. Note that, unlike MST, traditional radioisotope
235 binding assays are not accurate for low affinity interactions. Raw data with the quality control
236 parameters provided are in Fig 4 and S3 and are summarized in Table 1. The observed Kd of AtGPA1
237 binding GTP γ S was \sim 21 nM. This is within the range of Kds reported for animal G subunits (10-100
238 nM, (33)). XLG2 bound GTP γ S with a Kd of \sim 2 μ M which is 100 times lower affinity than GTP γ S binds
239 AtGPA1 when tested under the same conditions and nearly 1000 times lower when measured using
240 radioactive ligand (34). Moreover, the affinity of XLG2 to GDP is \sim 100 fold lower (177 μ M) than for
241 GTP γ S. Quantitative analyses clearly show that XLG2 is severely impaired in guanine nucleotide
242 binding (Table 1).

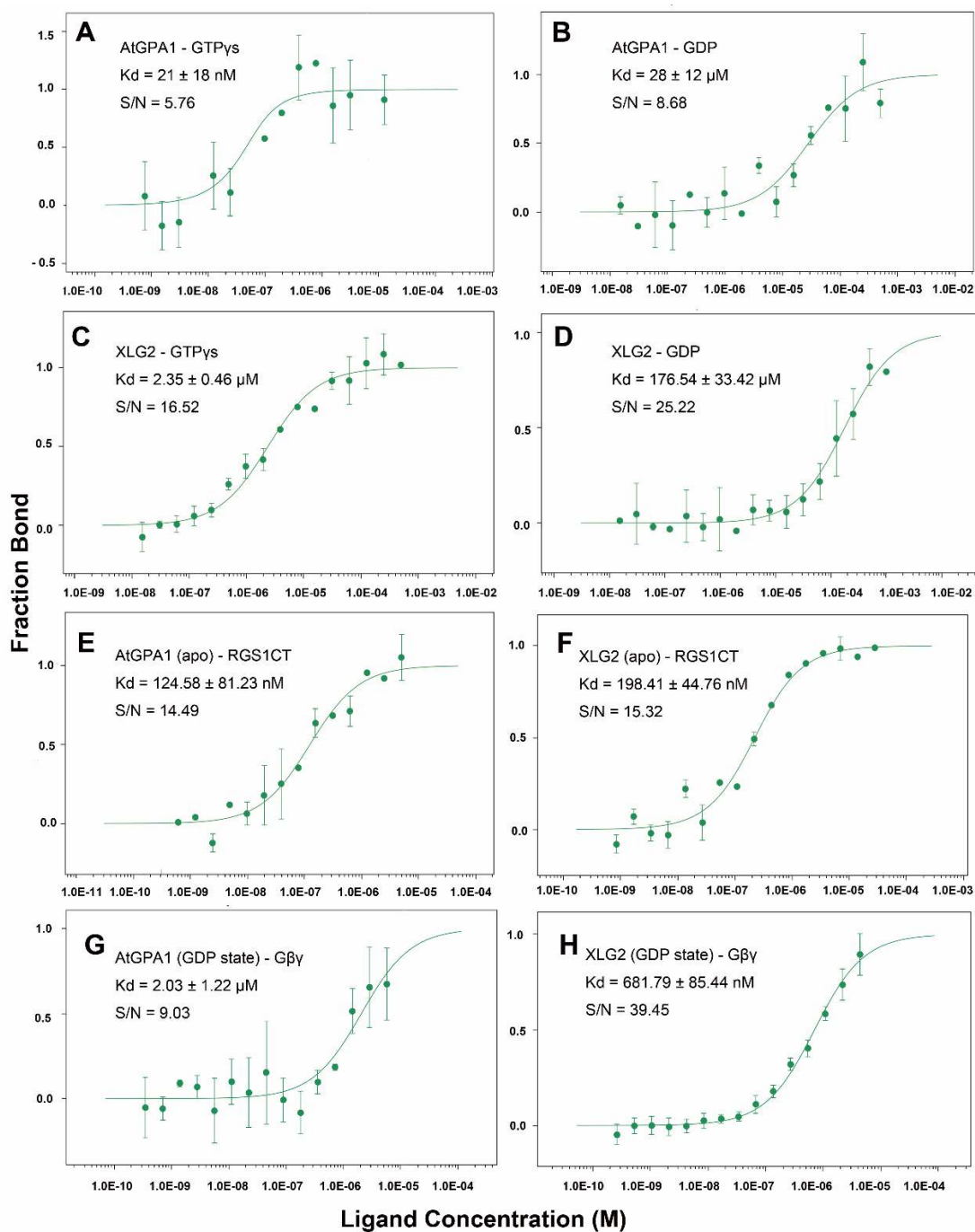
	GTP γ S	GDP	RGS1-C domain G α in apo state	RGS1-C domain G α in transition state	G $\beta\gamma$ G α in GDP state
AtGPA1	21 \pm 18 nM	28 \pm 12 μ M	125 \pm 81 nM	67 \pm 18 nM	2 \pm 1.22 μ M
XLG2	2350 \pm 460 nM	177 \pm 33 μ M	198 \pm 45 nM	NA	0.7 \pm 0.09 μ M

243

244

245
246
247
248

Table 1. Summary of the binding affinity (Kd) among AtGPA1 and XLG2 with nucleotide, RGS1-C domain and Gβγ. Top row in the inset indicates the tested interactors. The values were determined from the binding isotherms shown in Figure 4. The values are averages and StdDev for all the experimental replicates. Each experiment was replicated at least once.



249

250
251
252
253
254
255

Figure 4. Binding isotherms for nucleotide, RGS1-C domain and Gβγ to AtGPA1 and XLG2. Microscale Thermophoresis was used. (A) Binding isotherm and Kd value of AtGPA1 binding GTPγs and (B) GDP. (C) Binding isotherm and Kd value of XLG2 binding GTPγs and (D) GDP. (E) Binding isotherm and Kd value of RGS1 C terminal domain to AtGPA1 apo state and (F) XLG2 apo state. (G) Gβγ binding to AtGPA1 and (H) XLG2 Gα domain. S/N: signal to noise ratio. Each experiment was repeated at least once. Binding curve and Kd were fitted as described in Methods. Error bars represent StdDEV. Each experiment was repeated at least once.

256

257 With this poor affinity toward guanine nucleotides, the concentration of GTP in plant cells would
258 need to be 100 times greater than in animal cells for XLG2 to be GTP bound, however, for several
259 reasons, this explanation of a mechanism to compensate the weak GTP affinity by XLG proteins is not
260 reasonable. First, such a saturating concentration of GTP would eliminate the switch-like behavior of
261 the canonical plant G α subunit. Second, protein translation uses the same machinery in both plant and
262 animal cells and the GTP hydrolyzed for its proof reading and is sensitive to its cytoplasmic
263 concentration. Similarly, plant and animal microtubules requires GTP binding and hydrolysis. Both
264 translation and cytoskeletal dynamics would cease at this high concentration of GTP. Third, nucleotide
265 synthesis uses product inhibition to control the levels accordingly. A 100-fold higher concentration of
266 GTP would be incompatible with enzymes involved in nucleotide synthesis. Fourth, the highest known
267 concentration of GTP in plant cells is equivalent to only one Kd for GTP binding to XLG2 (35-37). As
268 such, the concentration of GTP in plant cells, especially non-dividing cells, may be rate-limiting for full
269 occupancy of XLG2 by GTP. For these reasons, we conclude that XLG2 is not likely bound by GTP *in*
270 *vivo*.

271 Assmann's group reported the unusual finding that the three XLG proteins bind and hydrolyze
272 GTP using Ca²⁺ instead of Mg²⁺ as a coordinating factor (32). To test this, we performed MST
273 experiments to measure the binding affinity of XLG2 with nucleotide in the presence of Ca²⁺. The results
274 showed lower binding affinity towards GTP γ S (~186 μ M) with Ca²⁺ vs. Mg²⁺ (Fig S3). This indicates that
275 Ca²⁺ may not act as the cofactor for XLGs binding GTP γ S. Ca²⁺ induced relatively higher binding affinity
276 for GDP (~28 μ M), albeit still poor, compared to Mg²⁺ as a cofactor (Fig S3).

277 Interestingly, despite XLG2 having much lower binding affinity towards GTP γ S and GDP
278 compared with AtGPA1, it had a similar binding affinity to the C-terminal RGS domain of AtRGS1 and
279 to the Arabidopsis G $\beta\gamma$ dimer (AGB1/AGG1). AtGPA1 bound AtRGS1 with a Kd ~125 nM with in
280 AtGPA1 in its apo state and ~ 67 nM in its transition state (Fig.S3). XLG2 has a similar Kd of ~198 nM

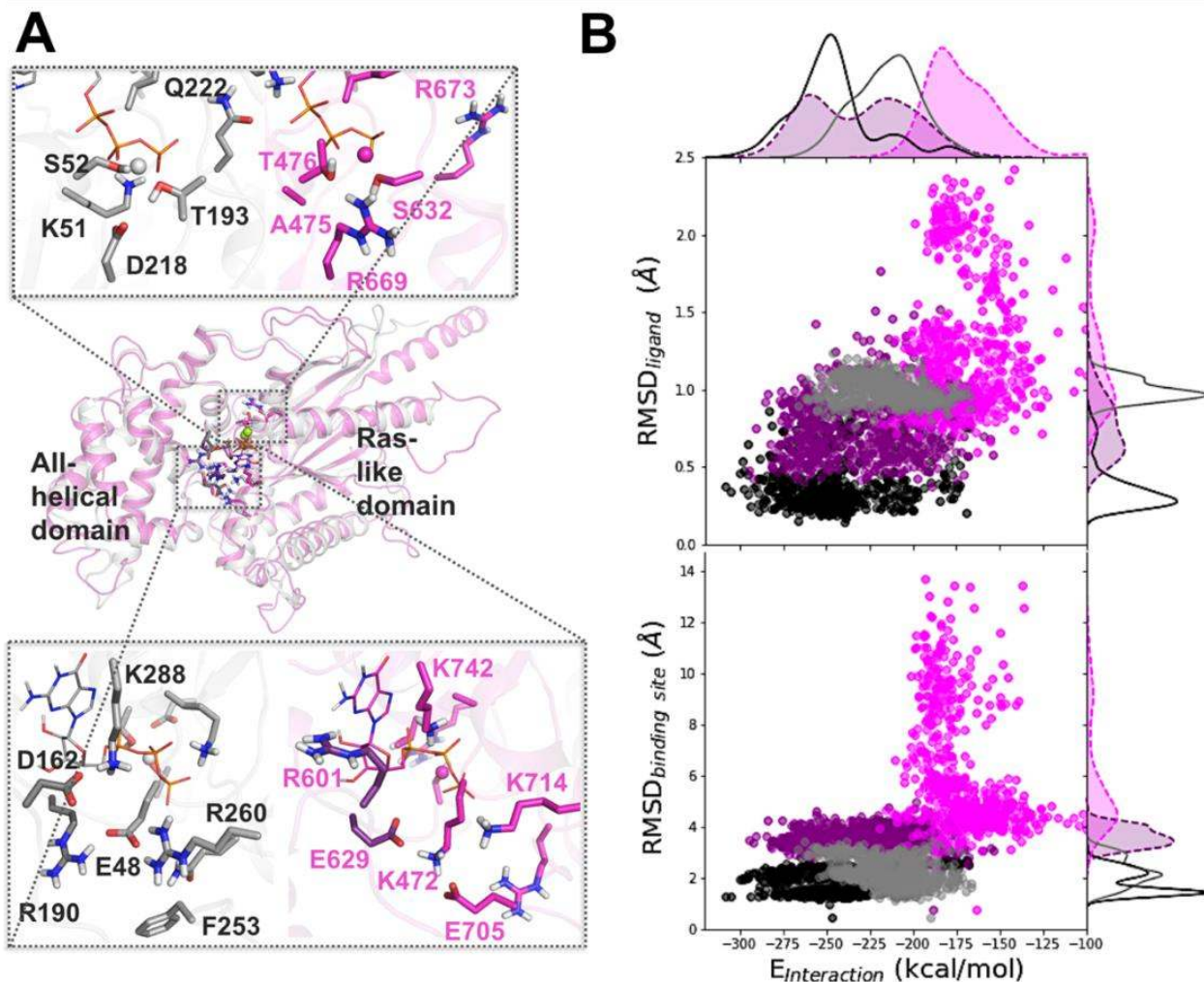
281 towards AtRGS1 when in its apo state (Table 1 and Fig. 4). The K_d for a transition state XLG2 was not
282 determined because this state is not relevant due to its nucleotide independence. Moreover, XLG2
283 showed a $\sim 0.7 \mu\text{M}$ binding affinity towards $G\beta\gamma$ similar to that of AtGPA1 which is $\sim 2 \mu\text{M}$ (Table 1 and
284 Fig. 4). This suggests that XLG2 exists as a nucleotide-independent inhibitor of G signaling through its
285 ability to sequester $G\beta\gamma$ directly or indirectly by binding to AtRGS1 thus enabling freed AtGPA1 to
286 sequester $G\beta\gamma$.

287 **A mechanistic explanation: Relative instability of XLG2 confers the reduced nucleotide** 288 **interaction**

289 We applied several computational modeling and simulation approaches to understand the underlying
290 molecular mechanisms differentiating AtGPA1 and XLG2 proteins. We sought to provide structural and
291 molecular dynamics rationales for the experimentally observed differences in nucleotide binding
292 preferences by the two proteins. To this point, we performed microseconds of molecular dynamics (MD)
293 simulations of four molecular complexes, involving GDP and GTP nucleotides, each in complex with
294 both AtGPA1 and the homology-modeled XLG2-1 $G\alpha$ domain, followed by comparative analyses of the
295 respective MD trajectories. The main finding of our simulations is that the molecular dynamic behaviors
296 of XLG2-1 differs from that of AtGPA1. We observed that overall XLG2-1 was more mobile in
297 comparison with AtGPA1, which generally retained its original crystallographic structure over the course
298 of simulations. Furthermore, to distinguish the two proteins with respect to their nucleotide binding
299 capabilities, we focused on analyzing the behavior of the ligand binding site both in the context of the
300 intra-protein and ligand-protein interactions in order to more clearly understand the key factors
301 contributing to the experimental findings of the lower nucleotide binding affinity in XLG2.

302 In preparation for MD simulations, the structure of XLG2 obtained by homology modeling, was
303 subjected to molecular mechanics minimization following several protocols as described in the Methods
304 section in order to avoid unnatural clashes between atoms resulting from homology modeling. To

305 understand the overall dynamics of the proteins, we analyzed RMS fluctuations per residue and
306 calculated RMSD using all C-alpha atoms of the proteins (**Fig. S4, S5**), which showed that the general
307 fold of AtGPA1 was more stable and the amino-acid residues displayed lower mobility compared to
308 XLG2. We then sought to understand the dynamics of the nucleotide binding site and explored the key
309 differences in the interactions formed within the binding site. First, we visualized the binding sites of the
310 two proteins to explore the main differences in terms of the amino-acid residue composition (**Fig. 5A**).
311 The following differences in the similarly-positioned, binding-site residues were determined between
312 AtGPA1 and XLG2: E48 to K472, D162 to R601, R190 to E629, F253 to E705, R260 to K714, K288 to
313 K742 in guanine and ribose binding sites, and K51 to A475, S52 to T476, T193 to S632, D218 to R669,
314 Q222 to R673 in Mg²⁺ and phosphates binding sites (**Fig. 1, 5**).



315

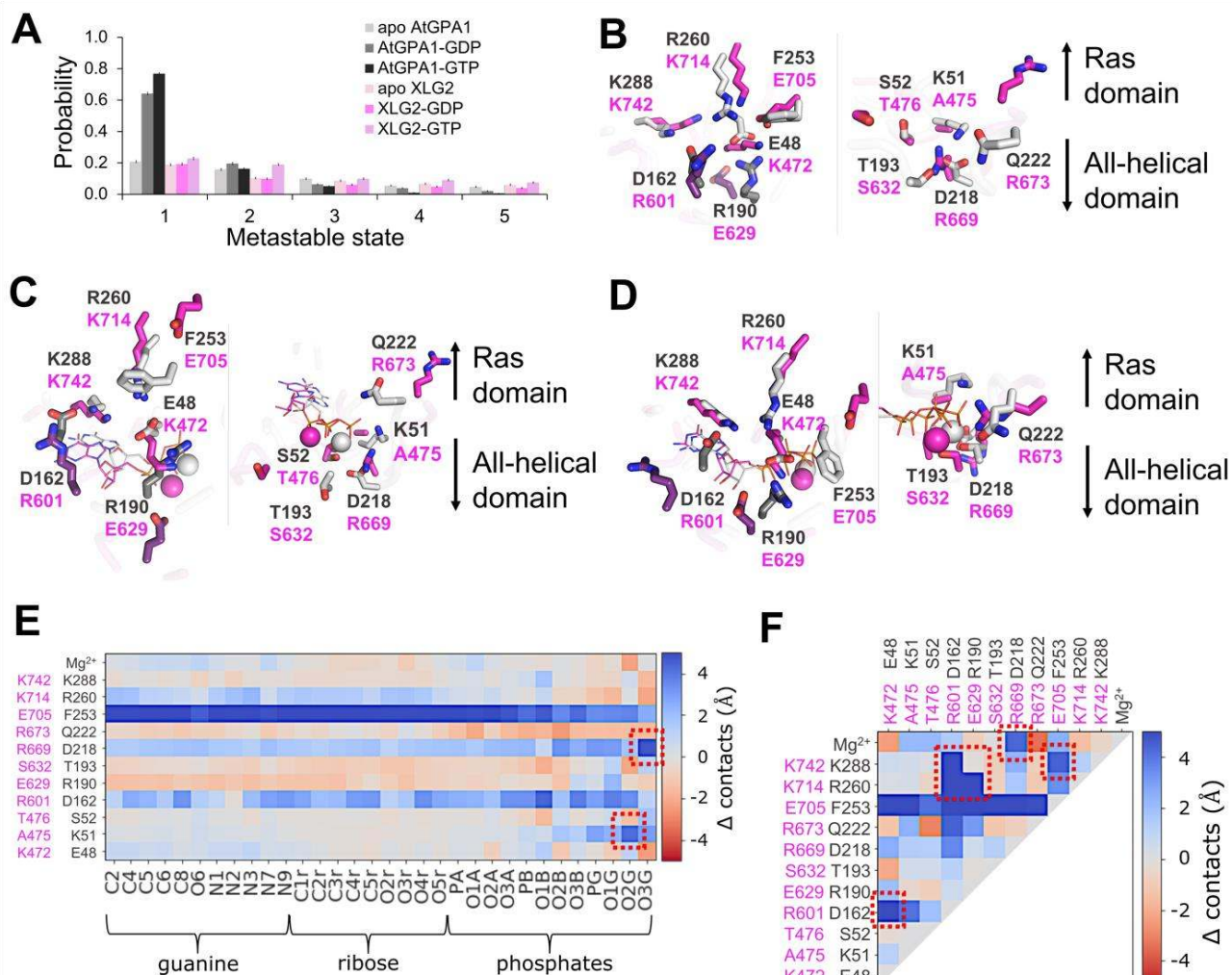
316 **Figure 5. Difference in dynamics between the nucleotide-bound AtGPA1 and XLG2: Insights from MD**
 317 **simulations.** Homology modeling and MD simulations reveal the main differences in amino-acid residue
 318 composition and the nucleotide binding site dynamics of AtGPA1 (grey) and XLG2 (magenta) **(A)** Aligned
 319 minimized AtGPA1 crystal structure (PDB ID 2xtz) and the homology modeled XLG2. The zoomed in plots
 320 separately display phosphate and Mg^{2+} binding site (top) and guanine and ribose binding site (bottom) on the
 321 example of GTP-bound complexes, highlighting the most prominent differences in the amino-acid residues. **(B)**
 322 The relationship between the nucleotide-protein interaction energies (designated as $E_{interaction}$ on the scatter plots,
 323 and calculated as the sum of the Coulomb and LJ terms) and mobility of the nucleotide ($RMSD_{ligand}$) and binding
 324 site ($RMSD_{binding\ site}$) display substantial separation among AtGPA1-GTP (black points and solid line), XLG2-GTP
 325 (purple points and dashed line), AtGPA1-GDP (grey points and solid line), and XLG2-GDP (pink points and
 326 dashed line) complexes (Fig. S6-8).

327

328 To understand the differences in the binding site dynamics, we first calculated RMSD of the heavy
 329 atoms of residues located in the binding sites (**Fig. 5B and Fig. S6**), which we defined as the protein
 330 residues within 4 Å from GTP (see Methods). We observed that AtGPA1 and XLG2 nucleotide binding

331 sites differed in conformational dynamics and had distinctly different configurations as elaborated in the
332 following paragraph. Next, we aimed to understand the impact of the difference in dynamics of the
333 binding site residues on the nucleotide mobility and nucleotide binding preferences (**Fig. 5B & Figs.**
334 **S7, S8**). Through exploring the relationship between the nucleotide-protein interaction energy
335 (calculated as the sum of intermolecular Coulomb and LJ terms of the molecular mechanics energy of
336 the nucleotide-protein complexes) and mobilities of the binding site and ligand, we observed substantial
337 differences across the four complexes formed when AtGPA1 and XLG2 bound to both GDP and GTP.
338 The molecular systems occupied distinct regions on each of these two landscapes. Importantly the
339 ranking order of the means of two parameters, (i) the nucleotide mobility in the pocket as characterized
340 by the RMSD of the nucleotide (from smallest to largest), and subsequently (ii) the nucleotide-protein
341 interaction energies characterized as the sum of all LJ and Coulomb terms of the nucleotide-
342 protein interactions (from more negative to less negative), agreed with the ranking order in terms of our
343 experimental binding affinities ($K_d \pm \text{StDev}$) as follows: **1st**) GPA1-GTP (0.021 \pm 0.018
344 μM), **2nd**) XLG2-GTP (2.4 \pm 0.5 μM), **3rd**) GPA1-GDP (28 \pm 12 μM), **4th**) XLG2-GDP (177 \pm 33
345 μM) (**Table 1**).

346 This result added confidence to our structural and simulations-derived interpretations of the
347 molecular complex formations. We would like to emphasize, however, that such calculations of the
348 intermolecular interaction energies are merely estimates of the relative strengths of ligand-protein
349 interactions in the bound state, which by no means is equivalent to the assessment of the change in
350 Gibbs free energy of binding (38-41).



351

352

353

354

355

356

357

358

359

360

361

362

363

364

365

366

367

368

369

370

371

372

Figure 6. Apo and nucleotide-bound proteins obtain distinct configurations defining the nucleotide binding preferences of AtGPA1 and XLG2. (A) The top five most populated metastable states of the nucleotide binding site obtained in cluster analysis of MD trajectories indicate that nucleotide-bound AtGPA1 obtains a stable frequently visited conformational state, whereas XLG2 complexes tend to transition between conformationally diverse states with lower probabilities. Interestingly, both apo proteins obtain multiple states with equivalently low probabilities (Fig. S6,S9). Aligned centroids of the largest metastable states are presented in panels B-D. (B) The most populous apo states show stable E48-R190-R260 and D162-K288 salt bridge networks in the guanine binding site (left image) of AtGPA1 (grey), and a more destabilized salt bridge network between similarly positioned residues in XLG2 (magenta) primarily contributed by R601-K742 electrostatic repulsion. K51-D218 salt bridge in the phosphate and Mg²⁺ binding sites (right image) enables a more structures AtGPA1, while the neutral A475 and a repulsion between R669 and R673 cause a more disintegrated XLG2. (C) GDP- and (D) GTP-bound complexes retain the strong salt bridge network in AtGPA1 and less stable electrostatic interactions in XLG2. K51 reorients and forms an additional bond with phosphates in AtGPA1, which is prevented by the equivalently positioned neutral A475 in XLG2. K472 breaks its bonds with E629 and re-arranges to interact with closer located phosphates. The absence of γ -phosphate in GDP makes the nucleotide more mobile, losing the frequency of its contacts. R673 in GTP-bound XLG2, however, forms a relatively stable bond with the γ -phosphate seemingly increasing the nucleotide binding affinity. The residues shown in darker shades in panels B-D (D162 and R190 of GPA1; R601 and E629 of XLG2) make the key intra-protein interactions defining the binding site shape. The differences in the frequency of the aforementioned interactions, on the example of GTP-bound complexes, are clearly seen through heatmaps of Δ contacts (minimum distances) (E) between the non-hydrogen atoms of the nucleotide and binding site residues, and (F) within the binding site

373 residues. 100 states of the most populated clusters were used to generate the heatmaps. The red squares
374 highlight the most prominent changes in the interactions stipulating the importance of the residues to the stability
375 of the active sites and to the interactions with the nucleotide.
376

377 Cluster analysis of the generated MD trajectories (42-44) (see Methods for details) revealed
378 metastable states with distinct configurations of the binding sites linked to the experimental nucleotide
379 binding preferences (**Fig. 6**). For the most populated metastable state of each molecular complex, we
380 explored the specific intra-protein chemical interactions which directly impact the dynamics of the active
381 sites, and their impact on the nucleotide-binding interactions. The results show that nucleotide-bound
382 AtGPA1 achieves stable dominant (i.e., frequently visited) conformations, whereas XLG2 complexes
383 tend to transition between conformationally-diverse states with lower probabilities. Such low frequency
384 populations of the top clusters are associated with a more dynamic binding pocket in XLG2.
385 Interestingly, both apo-proteins assume multiple states with low probabilities across the top five clusters
386 (**Fig. S6A, S9, Supplemental Movies 1-6**).

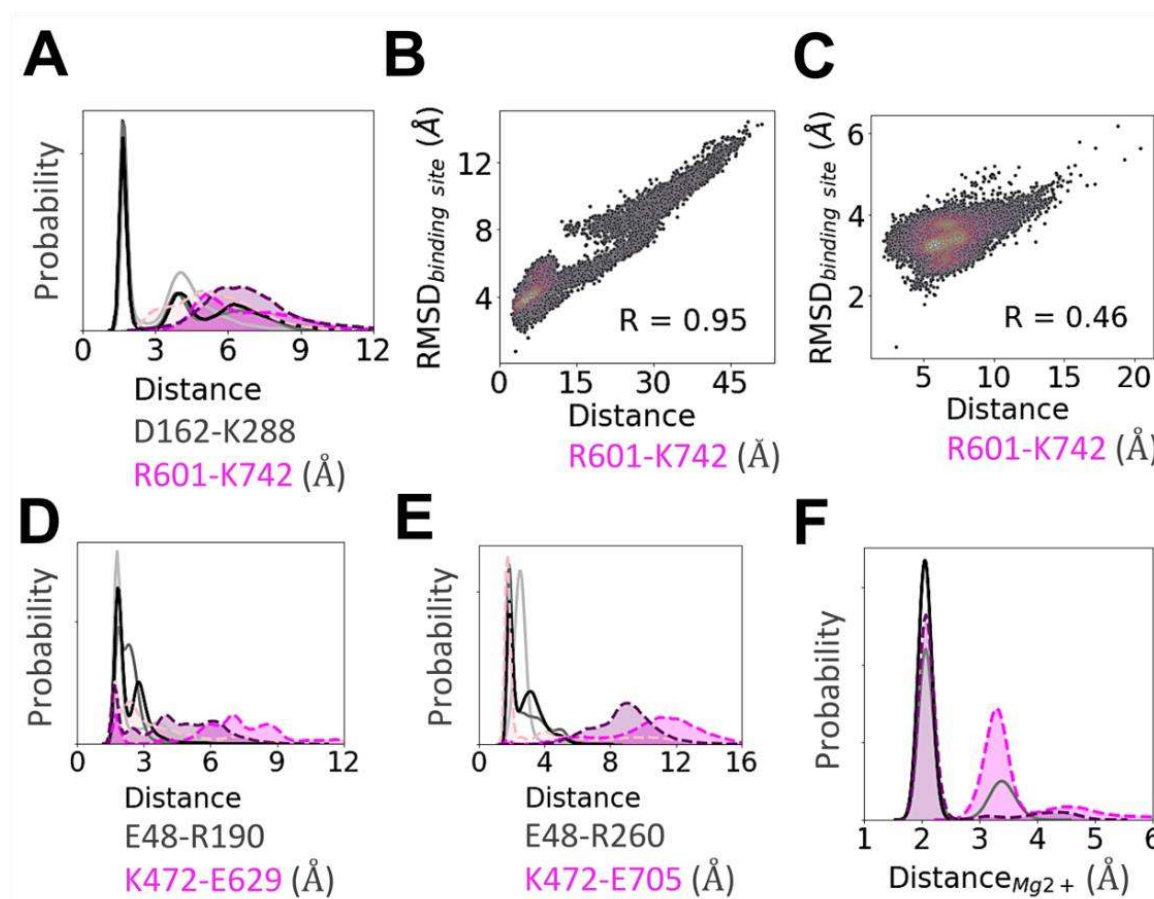
387 The most populous states of the apo-protein show a stable salt bridge network in AtGPA1, but
388 no network and fewer coherent salt bridges are found in XLG2-1. In the guanine binding site of AtGPA1,
389 salt bridges formed between E48 of the P-loop, R190 of Switch I, and R260 of Switch III, as well as
390 between D162 and K288, while a more destabilized salt bridge network appeared between similarly
391 positioned residues in XLG2-1, namely: E629 of Switch I, K472 of P-loop, K714 of Switch III and E705
392 (**Fig. 6B, S9-12**). In XLG2-1, a positive charge at K714 (position equivalent to R260 in AtGPA1) is not
393 capable of forming a salt bridge with K472 (position equivalent to E48 in AtGPA1). In the phosphate
394 and Mg²⁺ binding sites, the K51-D218 salt bridge enables a more structured apo-AtGPA1, while for
395 XLG2, the neutral sidechain of A475 (position equivalent to K51 in AtGPA1) together with a repulsion
396 between R669 and R673 precludes a stabilizing salt bridge. In general, AtGPA1 salt bridges formed by
397 the two loop residues D162 and R190 (and equivalently placed E629 in XLG2) drawing the two domains
398 closer together to subsequently increase the number of interactions between the all-helical domain and
399 the nucleotide.

400 The nucleotide-bound complexes retain the aforementioned strong salt bridge network in
401 AtGPA1 and weak electrostatic interactions in XLG2 (**Fig. 6C,D, Fig. S9-12**). In the bound state, the
402 K51 sidechain of AtGPA1 was re-arranged to form an additional bond with phosphates, which is an
403 additional salt bridge lacking by the neutral A475 in XLG2-1. In the GTP-bound XLG2-1 model, E705
404 lost its K472 interaction to γ -phosphate which also attracted R673 for further stabilization. Moreover,
405 E48 in AtGPA1 avoided the negatively-charged phosphates which further promoted electrostatic
406 interactions with both R190 and R260 to stabilize this cavity. In the GDP-occupied state, due to the lack
407 of the γ -phosphate, GDP is more mobile and loses a number of its contacts with the active site residues
408 in both $G\alpha$ proteins, but more so in XLG2-1 due its structurally-unstable binding site.

409 The heatmaps of Δ contacts from experiments determining the difference in the minimum
410 distances between the two $G\alpha$ proteins and **(i)** the atoms of the nucleotide and binding site residues,
411 and **(ii)** intra-protein interactions within the binding site residues, clearly show the contrast between the
412 interaction frequencies within these two proteins. As highlighted in Fig 6E and F, the most prominent
413 changes in the interactions important to the stability of the active sites and to the interactions with the
414 nucleotide, in addition to the previously indicated interactions, reside with F253 in AtGPA1 which was
415 overall closer to both the nucleotide and the binding site residues compared with similarly positioned
416 E705 in XLG2-1. This aromatic residue makes frequent pi-cation interactions with R190 in both apo-
417 and ligand-bound protein and occasional pi-cation interactions with the Mg^{2+} in the ligand-bound state.

418 Our analyses shows that the D162-K288 salt bridge (**Fig. 7A**) is one of the key interactions
419 maintaining the shape of the apo-AtGPA1 nucleotide-binding site. In contrast in XLG2-1, two positively
420 charged residues, R601 and K742, situated in positions equivalent to D162 and K288 of AtGPA1
421 caused electrostatic repulsion, pushing away the all-helical domain of the protein from the Ras-like
422 domain, resulting in an increased mobility and a less structured nucleotide binding site in XLG2-1. The
423 R601-K742 distance in XLG2-1 was highly correlated with the fluctuations of the binding site in XLG2-
424 GDP and to a lesser extent in XLG2-GTP (**Fig. 7B and C**). The reason for the former is the lack of an

425 extra anchor in terms of γ -phosphate in GDP to enable the electrostatic repulsion between R601 and
 426 K742 to be the main contributor to the instability of XLG2-GDP binding pocket. This agrees with the
 427 experimentally observed poor binding affinity of GDP to XLG2. Although this correlation still exists in
 428 XLG2-GTP, it is less pronounced due to the presence of the extra phosphate in GTP. In XLG2, K714
 429 makes ionic bonds with phosphates, however, this does not seem to be sufficient to retain the binding
 430 site integrity distorted by the aforementioned repulsion.



431

432 **Figure 7. Key intra-protein distances responsible for the experimental nucleotide binding affinities as**
 433 **determined from MD simulations.** Distribution of the minimum distances between the residues emphasized in
 434 Fig. 6 and text. In general, a stronger salt bridge network in AtGPA1 maintains the shape of its nucleotide-bound
 435 binding site (see text for more details). **(A)** Distance between D162 and K288 and the equivalently placed R601
 436 and K742 in XLG2. **(B)** The repulsion between R601 and K742 is highly correlated (R=0.95) with the binding site
 437 RMSD in XLG2-GDP and **(C)** to a lesser extent in XLG2-GTP (R=0.46). The 2D correlation plots were
 438 constructed using kernel-density estimation with Gaussian kernels. **(D)** Distance between E48 and R190 in
 439 AtGPA1 and similarly positioned K472 and E629. **(E)** Distance between E48 and R260 in AtGPA1 and K472
 440 and E705 (aligned with F253 of AtGPA1) in XLG2. The distributions show that both of the salt bridges (panels
 441 E and D) are dominant in the apo proteins, and are less persistent in nucleotide-bound XLG2. **(F)** The
 442 distributions of the minimum distance between Mg²⁺ and γ -phosphate binding site residues (D218, S52, T193,
 443 and D218 in GPA1; T476, S632, R669 in XLG2) and Mg²⁺ counterion. For clarity in panels A, D, E, and F the

444 values of probabilities on the y-axis are hidden. Apo AtGPA1 is plotted with solid light grey lines, AtGPA1-GDP—
445 solid grey, AtGPA1-GTP—solid black, apo XLG2—dotted pink, XLG2-GDP—dotted magenta, XLG2-GTP—
446 dotted purple; the probability densities for XLG2 are shaded for contrast.

447
448 Another distinction between the two proteins is in the Mg^{2+} binding site (**Fig. 7F & Fig. S13**)
449 discussed above. In AtGPA1, D218 formed an H-bond with S52 (which interacts with Mg^{2+}) and a
450 Coulomb interaction with Mg^{2+} , whereas the ‘bulkier’ and positively charged sidechain of R669 in XLG2
451 (position equivalent to D218 in AtGPA1) did not form stable interactions with either T476 or S632 (which
452 interact with Mg^{2+}) and caused an electrostatic repulsion with Mg^{2+} . The distribution of the minimum
453 distance between the Mg^{2+} binding site residues (S52, T193, D218, and Q222 in AtGPA1; T476, S632,
454 R669, and R673 in XLG2) and the Mg^{2+} counterion clearly explain this effect.

455 To interpret the observed equivalent AtRGS1 binding capability of the two Gα proteins (**Fig. 3,**
456 **4, Table 1**), we estimated the structural stability of the specific regions that are involved in AtRGS1
457 binding (**Fig. S14**). We showed that the three equivalently placed AtRGS1 binding site residues of apo-
458 AtGPA1 and apo-XLG2-1 similarly maintained their structural integrity over the course of our
459 simulations. Such conformationally-preserved regions in the apo-proteins position them to bind AtRGS1
460 when it is tethered close to either protein.

463 **Conclusion**

464 XLG2 binds GTP *in vitro* poorly such that at the estimated concentration of GTP in plant cells, XLG2 is
465 not expected to be nucleotide bound. However, XLG2 binds regulatory partners, AtRGS1 and G $\beta\gamma$.
466 Therefore, XLG2 is a decoy that negatively regulates by sequestering the G $\beta\gamma$ dimer directly and also
467 indirectly by promoting AtGPA1 interacting with G $\beta\gamma$ through freeing AtGPA1 from the
468 AtRGS1::AtGPA1 complex. While this concept shares similarities for control of G signaling by dominant
469 negative mutations of canonical G protein in animals (45), it is unique in that the negative control is
470 provided *in trans* by a genetically-encoded, atypical G protein.

471 Taken together, our modeling data provide credible interpretations for the experimentally
472 observed strengths of guanine nucleotide binding to AtGPA1 and XLG2. Several key intra-protein and
473 nucleotide-protein interactions in AtGPA1 were shown to be attributed to the higher structural stability
474 of the binding site of the protein and to more persistent contacts of the protein with the nucleotide and
475 magnesium. We show mechanistically that among the chief intra-protein interactions preserving the
476 stability of the binding site in both apo- and nucleotide-bound-states of AtGPA1 include the following
477 ionic bonds: D162-K288, R190-E48-R260, and K51-D218. Because XLG2 is important for disease
478 resistance and development (17, 46, 47), engineering these equivalent residues may lead to
479 improvements in crop performance.

482 **Acknowledgments**

483 This work was supported by NIGMS (R01GM065989) and NSF (MCB-0718202) awarded to Alan. M. Jones.
484 The deep computational analyses were supported by the resources of the UNC Longleaf cluster
485 (<https://its.unc.edu/research-computing/longleaf-cluster/>)
486
487

488 References

489

- 490 1. Lambert NA (2008) Dissociation of heterotrimeric G proteins in cells. *Sci Signal* 1(25):re5.
- 491 2. Sprang SR (1997) G proteins, effectors and GAPs: structure and mechanism. *Current Opinion in Structural Biology*
- 492 7(6):849-856.
- 493 3. Urano D, Chen J-G, Botella JR, & Jones AM (2013) Heterotrimeric G protein signalling in the plant kingdom. *Open*
- 494 *Biology* 3(3).
- 495 4. Urano D & Jones AM (2014) Heterotrimeric G protein-coupled signaling in plants. *Annual Review of Plant*
- 496 *Biology* 65(1):365-384.
- 497 5. Kleuss C, Raw AS, Lee E, Sprang SR, & Gilman AG (1994) Mechanism of GTP hydrolysis by G-protein alpha
- 498 subunits. *Proc Natl Acad Sci U S A* 91(21):9828-9831.
- 499 6. Sprang SR (2016) Invited review: Activation of G proteins by GTP and the mechanism of Galpha-catalyzed GTP
- 500 hydrolysis. *Biopolymers* 105(8):449-462.
- 501 7. Sprang SR (1997) G protein mechanisms: insights from structural analysis. *Annu Rev Biochem* 66:639-678.
- 502 8. Gilman AG (1987) G proteins: transducers of receptor-generated signals. *Annu Rev Biochem* 56:615-649.
- 503 9. Temple BR, Jones CD, & Jones AM (2010) Evolution of a signaling nexus constrained by protein interfaces and
- 504 conformational States. (Translated from eng) *PLoS computational biology* 6(10):e1000962 (in eng).
- 505 10. Jones JC, *et al.* (2011) The crystal structure of a self-activating G protein alpha subunit reveals its distinct
- 506 mechanism of signal initiation. *Sci Signal* 4(159):ra8.
- 507 11. Chakravorty D, Gookin TE, Milner MJ, Yu Y, & Assmann SM (2015) Extra-Large G proteins expand the repertoire
- 508 of subunits in Arabidopsis heterotrimeric G protein signaling. *Plant Physiology* 169(1):512-529.
- 509 12. Ullah H, Chen J-G, Temple B, Boyes D, & Alonso J (2003) The β subunit of the Arabidopsis G protein negatively
- 510 regulates auxin-induced cell division and affects multiple developmental processes. *Plant Cell* 15:393.
- 511 13. Thung L, Trusov Y, Chakravorty D, & Botella J (2012) G γ 1 + G γ 2 + G γ 3 = G β : The search for heterotrimeric G-
- 512 protein γ subunits in Arabidopsis is over. *J. Plant Physiol.* 169:542.
- 513 14. Johnston CA, *et al.* (2007) GTPase acceleration as the rate-limiting step in Arabidopsis G protein-coupled sugar
- 514 signaling. *Proceedings of the National Academy of Sciences* 104(44):17317-17322.
- 515 15. Maruta N, Trusov Y, Brenya E, Parekh U, & Botella JR (2015) Membrane-localized extra-large G proteins and G $\beta\gamma$
- 516 of the heterotrimeric G proteins form functional complexes engaged in plant immunity in Arabidopsis. *Plant*
- 517 *Physiology* 167(3):1004-1016.
- 518 16. Urano D, *et al.* (2016) Saltatory evolution of the heterotrimeric G protein signaling mechanisms in the plant
- 519 kingdom. *Science Signaling* 9(446): ra93.
- 520 17. Liang X, *et al.* (2018) Ligand-triggered de-repression of Arabidopsis heterotrimeric G proteins coupled to
- 521 immune receptor kinases. *Cell Research* 28(5):529-543.
- 522 18. Urano D, *et al.* (2016) Plant morphology of heterotrimeric G protein mutants. *Plant and Cell Physiology*
- 523 57(3):437-445.
- 524 19. Coleman DE, *et al.* (1994) Structures of active conformations of Gi alpha 1 and the mechanism of GTP hydrolysis.
- 525 *Science* 265(5177):1405-1412.
- 526 20. Berman DM, Wilkie TM, & Gilman AG (1996) GAIP and RGS4 are GTPase-activating proteins for the Gi subfamily
- 527 of G protein alpha subunits. *Cell* 86(3):445-452.
- 528 21. Jones JC, Jones AM, Temple BR, & Dohlman HG (2012) Differences in intradomain and interdomain motion
- 529 confer distinct activation properties to structurally similar Galpha proteins. *Proc Natl Acad Sci U S A*
- 530 109(19):7275-7279.
- 531 22. Jones JC, Temple BR, Jones AM, & Dohlman HG (2011) Functional reconstitution of an atypical G protein
- 532 heterotrimer and regulator of G protein signaling protein (RGS1) from Arabidopsis thaliana. *J Biol Chem*
- 533 286(15):13143-13150.
- 534 23. Saraste M, Sibbald PR, & Wittinghofer A (1990) The P-loop--a common motif in ATP- and GTP-binding proteins.
- 535 *Trends Biochem Sci* 15(11):430-434.

- 536 24. Seeburg PH, Colby WW, Capon DJ, Goeddel DV, & Levinson AD (1984) Biological properties of human c-Ha-ras1
537 genes mutated at codon 12. *Nature* 312(5989):71-75.
- 538 25. Bosch DE, *et al.* (2012) A P-loop mutation in Galpha subunits prevents transition to the active state: implications
539 for G-protein signaling in fungal pathogenesis. *PLoS Pathog* 8(2):e1002553.
- 540 26. Raw AS, Coleman DE, Gilman AG, & Sprang SR (1997) Structural and biochemical characterization of the
541 GTPgammaS-, GDP.Pi-, and GDP-bound forms of a GTPase-deficient Gly42 --> Val mutant of Gialpha1.
542 *Biochemistry* 36(50):15660-15669.
- 543 27. Noel JP, Hamm HE, & Sigler PB (1993) The 2.2 Å crystal structure of transducin-alpha complexed with GTP
544 gamma S. *Nature* 366(6456):654-663.
- 545 28. Barren B & Artemyev NO (2007) Mechanisms of dominant negative G-protein alpha subunits. *J Neurosci Res*
546 85(16):3505-3514.
- 547 29. Lee E, Taussig R, & Gilman AG (1992) The G226A mutant of Gs alpha highlights the requirement for dissociation
548 of G protein subunits. *J Biol Chem* 267(2):1212-1218.
- 549 30. Posner BA, Mixon MB, Wall MA, Sprang SR, & Gilman AG (1998) The A326S mutant of Gialpha1 as an
550 approximation of the receptor-bound state. *J Biol Chem* 273(34):21752-21758.
- 551 31. Iiri T, Herzmark P, Nakamoto JM, van Dop C, & Bourne HR (1994) Rapid GDP release from Gs alpha in patients
552 with gain and loss of endocrine function. *Nature* 371(6493):164-168.
- 553 32. Heo JB, Sung S, & Assmann SM (2012) Ca²⁺-dependent GTPase, Extra-large G Protein 2 (XLG2), promotes
554 activation of DNA-binding protein related to Vernalization 1 (RTV1), leading to activation of floral integrator
555 genes and early flowering in Arabidopsis. *Journal of Biological Chemistry* 287(11):8242-8253.
- 556 33. Malinski JA, Zera EM, Angleson JK, & Wensel TG (1996) High affinity interactions of GTPγS with the
557 heterotrimeric G Protein, transducin: Evidence at high and low protein concentrations *J Biol Chem*
558 271(22):12919-12924.
- 559 34. Johnston CA, Willard MD, Kimple AJ, Siderovski DP, & Willard FS (2008) A sweet cycle for Arabidopsis G-proteins:
560 Recent discoveries and controversies in plant G-protein signal transduction. *Plant Signal Behav* 3(12):1067-1076.
- 561 35. Ashihara H & Nygaard P (1989) Purine nucleotide and RNA synthesis in suspension cultured cells of carrot.
562 *Physiologia Plantarum* 75:31-36.
- 563 36. Meyer R & Wagner KG (1985) Analysis of the nucleotide pool during growth of suspension cultured cells of
564 *Nicotiana tabacum* by high performance liquid chromatography. *Physiologia Plantarum* 65(4):439-445.
- 565 37. Yin Y, Katahira R, & Ashihara H (2014) Metabolism of purine nucleosides and bases in suspension-cultured
566 *Arabidopsis thaliana* cells. *Eur. Chem. Bull.* 3(9):925-934.
- 567 38. Ganotra GK & Wade RC (2018) Prediction of Drug-Target Binding Kinetics by Comparative Binding Energy
568 Analysis. *ACS Med Chem Lett* 9(11):1134-1139.
- 569 39. Henriksen NM, Fenley AT, & Gilson MK (2015) Computational Calorimetry: High-Precision Calculation of Host-
570 Guest Binding Thermodynamics. *J Chem Theory Comput* 11(9):4377-4394.
- 571 40. Mobley DL & Gilson MK (2017) Predicting Binding Free Energies: Frontiers and Benchmarks. *Annu Rev Biophys*
572 46:531-558.
- 573 41. Fujitani H, *et al.* (2005) Direct calculation of the binding free energies of FKBP ligands. *J Chem Phys*
574 123(8):084108.
- 575 42. Abramyan TM, Snyder JA, Thyparambil AA, Stuart SJ, & Latour RA (2016) Cluster analysis of molecular simulation
576 trajectories for systems where both conformation and orientation of the sampled states are important. *Journal*
577 *of Computational Chemistry* 37(21):1973-1982.
- 578 43. Daura X, *et al.* (1999) Peptide folding: When simulation meets experiment. *Angewandte Chemie International*
579 *Edition* 38(1-2):236-240.
- 580 44. Shao J, Tanner S, Thompson N, & Cheatham T (2007) Clustering molecular dynamics trajectories: 1.
581 Characterizing the performance of different clustering algorithms. *J Chem Theory Comput.* 3(6):2312-2334.
- 582 45. Barren B & Artemyev NO (2007) Mechanisms of dominant negative G-protein α subunits. *Journal of*
583 *Neuroscience Research* 85(16):3505-3514.
- 584 46. Liang X, *et al.* (2016) Arabidopsis heterotrimeric G proteins regulate immunity by directly coupling to the FLS2
585 receptor. *eLife* 5:e13568.

- 586 47. Liang Y, Gao Y, & Jones AM (2017) Extra large G-Protein interactome reveals multiple stress response function
587 and partner-dependent XLG subcellular localization. *Frontiers in Plant Science* 8(1015).
588
589
590